

1 **The secondary chemistry of synthetic fuel oxymethylene**
2 **ethers unraveled: Theoretical and kinetic modeling of**
3 **methoxymethyl formate and formic anhydride decomposition**

4 Kevin De Ras^a, Mike Bonheure^a, Joris W. Thybaut^a, Kevin M. Van Geem^{a,*}

5

6 ^a *Laboratory for Chemical Technology (LCT), Ghent University, Technologiepark 125,*
7 *B-9052 Ghent, Belgium*

8

9 *Corresponding author.

10 *E-mail address:* Kevin.VanGeem@UGent.be (Kevin M. Van Geem)

11

12

13 **HIGHLIGHTS**

- 14 • Study on the decomposition of methoxymethyl formate (MMF) and formic
15 anhydride (FA)
- 16 • MMF and FA are formed during pyrolysis and oxidation of oxymethylene ethers
- 17 • Development of a new kinetic model with detailed MMF and FA chemistry
- 18 • Thermodynamic and kinetic parameters based on first principles
- 19 • MMF and FA are more reactive compared to oxymethylene ether analogues

20

ABSTRACT

Replacing fossil fuels by oxymethylene ethers (OMEs) produced from renewable resources could help to reduce the rising CO₂ levels. In this work, the thermal decomposition chemistry of methoxymethyl formate (CH₃OCH₂OCHO) and formic anhydride (OCHOCHO) is investigated by means of a combination of quantum chemical calculations and kinetic modeling. The latter compounds are two important intermediates formed during the thermal decomposition chemistry of synthetic fuel OMEs. Two detailed kinetic models are developed based on first principles to describe the radical decomposition chemistry of methoxymethyl formate and formic anhydride, which are ultimately incorporated into the OME-2 model from De Ras et al. (Combustion and Flame, 2022). This newly obtained kinetic model describes experimental measurements for pyrolysis from literature significantly better than the model from the original study, without any fitting of thermodynamic or kinetic parameters. More particularly, some minor compounds are now satisfactorily reproduced within the experimental uncertainty margin of 10 mol% relative. Methoxymethyl formate and formic anhydride are found to be more reactive compared to OMEs. Both a reaction pathway analysis and sensitivity analysis reveal the important decomposition pathways under pyrolysis conditions.

Keywords: Oxymethylene ether, Methoxymethyl formate, Formic anhydride, Thermal decomposition chemistry, Automatic kinetic modeling.

1. Introduction

A lot of research is ongoing to replace fossil fuels with new (liquid) energy carriers, which can be produced in a sustainable manner, preferably using renewable energy [1]. Polyoxymethylene dimethyl ethers (PODEs), better known as oxymethylene ethers (OMEs), with structural formula $\text{CH}_3\text{O}(\text{CH}_2\text{O})_n\text{CH}_3$ (OME- n) represent a family of synthetic fuel molecules with very promising combustion characteristics [2]. These OMEs can contribute to the development of a circular carbon economy when produced from captured carbon monoxide and/or carbon dioxide and renewable electricity [3, 4]. Moreover, several internal combustion engine studies have already demonstrated that OMEs also significantly reduce the particulate matter emissions when used as an alternative or additive to conventional diesel fuels [5-8]. However, fundamental insight into both the pyrolysis and combustion chemistry remains a prerequisite to the introduction of OMEs on a global scale as a sustainable alternative for conventional fossil fuels.

In previous work, De Ras et al. [9] demonstrated the formation of methyl formate (MF, CH_3OCHO), methoxymethyl formate (MMF, $\text{CH}_3\text{OCH}_2\text{OCHO}$) and formic anhydride (FA, OCHOCHO) as important intermediates during OME pyrolysis and combustion. Several experimental and theoretical studies have already been performed to unravel the details of both the pyrolysis and combustion of MF [10-13]. Meanwhile, this decomposition chemistry has been included in multiple base mechanisms such as AramcoMech 1.3 [14] and CRECK [15]. This is in contrast with the chemistry of MMF and FA for which no such experimental and theoretical studies are available in the literature. Nevertheless, the decomposition chemistry of these compounds has already been included partly in kinetic models for OME pyrolysis and combustion, e.g., the models from Cai et al. [16], De Ras et al. [9], He et al. [17] and Sun et al. [18]. This

inclusion is mainly based upon analogies from alkanes, OMEs and MF, which are, however, found to lead to large discrepancies up to an order of magnitude between model predicted yields and experimental measurements. Therefore, in this new study, thermodynamic parameters and reaction rate coefficients have been determined for MMF and FA from quantum chemical calculations for the first time.

In this study, a new elementary step kinetic model, containing thermodynamic and kinetic parameters determined with electronic structure calculations at the CBS-QB3 level of theory, is developed which describes in detail the pyrolysis and combustion chemistry of MMF and FA. Due to the scarcity of experimental data and the fact that it is simply impossible to obtain MMF and FA as pure products, the validation is carried out by comparison against pyrolysis experiments with OME-2 in a tubular quartz reactor during which MMF is formed and could be carefully quantified. Rapid compression machine (RCM) experiments with OME-2/air mixtures are simulated for validation of the oxidation chemistry. Reaction pathway and sensitivity analyses unravel the most important decomposition pathways for both molecules under pyrolysis conditions.

2. Methodology

2.1. Computational methodology

All quantum chemical calculations are performed on the high-performance computing infrastructure of Ghent University at the CBS-QB3 level of theory [19] as implemented in the Gaussian 16 software package [20].

The lowest energy conformer is extensively searched via optimization of the most likely structures combined with 1-dimensional rotational scans around each internal bond [21]. Thermodynamic parameters, i.e., the standard enthalpy of formation at 298 K (ΔH_f^{298K}), the standard intrinsic entropy at 298 K (S^{298K}) and specific heat capacities

at several temperatures (C_p), are calculated by applying the principles of ideal gas statistical thermodynamics to the results of the optimized geometries of stable species and transition states. In the case of multiple stereoisomers for a molecule, only the one corresponding with the lowest electronic energy is retained. The internal modes are treated as harmonic oscillators except for modes associated with rotations around a single bond. The latter are approximated by 1-dimensional hindered internal rotations calculated at the B3LYP/6-31G(d) level of theory if the electronic barrier does not exceed 100 kJ mol⁻¹. The Fourier series expression of the rotational hindrance potential together with the reduced moment of inertia at the I^(2,3) level, as defined by East et al. [22], are used to construct the Schrödinger equation for 1-dimensional internal rotation. The eigenvalues of the solution are used to determine the partition function as a function of the temperature. Thermodynamic parameters are derived from the total partition function considering additionally the molecular symmetry and the number of optical isomers (enantiomers). The atomization method is used to calculate the enthalpy of formation at 298 K. The latter is corrected with spin-orbit corrections (SOCs) [23] and empirical bond additive corrections (BACs) [24, 25] to account for systematic deviations between the calculated and experimentally measured values. SOCs and BACs are not applied in the case only relative formation enthalpies are required, i.e., for the calculation of reaction rate coefficients and the construction of potential energy surfaces. Classical transition state theory is used to calculate the high-pressure limit reaction rate coefficients over a temperature range from 300 to 2000 K, with the asymmetric Eckart potential to account for quantum chemical tunneling [26]. Based on our experience, high-pressure limit reaction rate coefficients are valid for most practical applications and do not require the master equation to be solved [27]. Modified Arrhenius parameters (A , n , E_a), as defined in Eq. (1) with $k(T)$ the reaction rate

coefficient, T the absolute temperature and R the universal gas constant, are determined via linear least-squares regression over the same temperature range.

$$k(T) = A \cdot \left(\frac{T}{1\text{ K}}\right)^n \cdot \exp\left(-\frac{E_a}{RT}\right) \quad (1)$$

With this methodology, the enthalpies of formation are assumed to be calculated within 4 kJ mol⁻¹ (defined as chemically accurate) and the reaction rate coefficients within a factor of 2 to 4, in accordance with previous studies [9, 28-30]. A list containing all new thermodynamic and kinetic parameters calculated at the CBS-QB3 level of theory is provided in the Supplementary Material. Geometrical structures of the species and transition states are provided as well.

2.2. Automatic kinetic model development

Two separate elementary step kinetic models are developed for the pyrolysis and combustion of MMF and FA with the in-house developed automatic kinetic model generation code ‘Genesys’ [31]. Subsequently, these two sub-models are included in the OME-2 seed model developed in previous work [9] also containing thermodynamic and kinetic parameters at the CBS-QB3 level of theory. All newly implemented species in the final model have thermodynamic parameters obtained from quantum chemical calculations. In the case of conflicting thermodynamic and/or kinetic parameters, the parameters of the new sub-models are selected. Furthermore, several kinetic parameters related to MF have been updated with new quantum chemical results. The reaction families, which describe the molecular rearrangements to go from reactant(s) to product(s) by means of an elementary reaction step, implemented into the model are (intramolecular) hydrogen abstractions, radical additions (including addition to molecular oxygen), the typical low-temperature oxidation chemistry similar to hydrocarbons and several new unimolecular decomposition pathways. Only for the addition of carbon-centered radicals to molecular oxygen, rate rules have been used

which were regressed by Cai et al. [32] based on a dataset with hydrocarbons. The thermodynamic consistency in the model is ensured by implementing the reactions as being reversible, except for reactions forming three or more products. Unlimited extension of the reaction mechanism is prevented by a rule-based criterion both on the level of the reaction products and reaction families, e.g., interactions between carbon-carbon bond species and OMEs are omitted. Moreover, the addition of hydroperoxy alkyl radicals to molecular oxygen is not included. The latter would require additional computational expensive calculations, which are redundant to accurately describe the oxidation chemistry [9, 16].

The extended kinetic model for pyrolysis and combustion of OME-2, containing 323 species (22 new) and 2522 reactions (271 new), is available in the Supplementary Material in CHEMKIN format.

2.3. Kinetic model simulations

The newly developed kinetic model is validated against experimental pyrolysis data for OME-2 from a micro-pyrolysis unit with a tubular quartz reactor. Reactor simulations are performed using the CHEMKIN PRO software [33] with the original and newly developed model for comparison. The reactor is simulated with an ideal plug flow reactor (PFR) model. The experimentally measured temperature profiles, mass flow rates, and pressure are used as input for the PFR model in line with the original study [9]. The reactor pressure is sufficiently high (i.e., 0.34 MPa) to be sure that the high-pressure limit reaction rate coefficients are valid. The simulation results of the kinetic model for oxidation experiments in an RCM are provided in the Supplementary Material.

3. Results and discussion

3.1. Initiation and decomposition chemistry

The pyrolysis and combustion chemistry of MMF and FA is like MF driven by free radicals. Radicals originate from homolytic bond scissions and, in the case of combustion, via hydrogen abstractions by molecular oxygen. In Fig. 1, the bond dissociation energies (BDE) at 0 K of the different chemical bonds in MMF and FA are depicted as calculated at the CBS-QB3 level of theory. For comparison, the calculated BDEs of MF are also shown. The nomenclature used in this work is indicated in the skeletal notation. The spatial geometry of FA is planar, but the molecule is not symmetrical due to the repulsive interactions between both carbonyl functionalities. The backbone of MMF is non-planar due to sp^3 -hybridized carbon atoms and has gauche interactions in the lowest energy conformer.

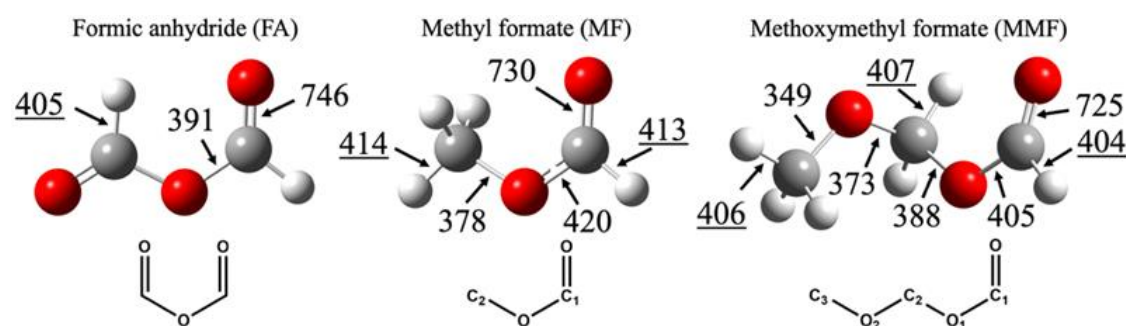


Fig. 1. Bond dissociation energies (BDE) at 0 K in kJ mol^{-1} for formic anhydride (FA), methyl formate (MF) and methoxymethyl formate (MMF) calculated at the CBS-QB3 level of theory. BDEs for carbon-hydrogen bonds are underlined for clarity. The used nomenclature for atoms in this work is indicated in the skeletal notation.

The $\text{C}_3\text{-O}_2$ bond with 349 kJ mol^{-1} and the C-O bond with 391 kJ mol^{-1} are the weakest in MMF and FA, respectively. For comparison, the $\text{C}_2\text{-O}$ bond is the weakest in MF with 378 kJ mol^{-1} . The introduction of a carbonyl functionality significantly impacts the chemical properties, as seen from the difference in BDE of 56 kJ mol^{-1} between $\text{C}_3\text{-O}_2$ and $\text{C}_1\text{-O}_1$ within MMF. The C-O bonds in MF are all about 10 to 15 kJ mol^{-1} stronger compared to the MMF equivalent. The $\text{C}_1\text{-H}$ is the weakest C-H bond in

MMF amounting to 404 kJ mol⁻¹. The other C-H BDEs in MMF, however, only differ by 3 kJ mol⁻¹ at most, despite the different chemical structure of all associated carbon-centered radicals. The BDE of the C-H bonds in FA is very similar amounting to 405 kJ mol⁻¹. These bonds are weaker than the two C-H bonds in MF, which amount to 413 and 414 kJ mol⁻¹. In contrast to the C-H bonds, the strength of the C=O bond in MMF is similar to the one in MF, while the bond in FA is 21 kJ mol⁻¹ stronger. The strength of the C-O bond is significantly affected by the presence of a carbonyl functionality, which is not the case for the C-H bonds.

The potential energy surfaces constructed for the possible radicals originating from MMF and FA are depicted and thoroughly discussed in the Supplementary Material. This includes the thermal decomposition pathways via β -scissions and intramolecular hydrogen abstractions (isomerizations).

It was concluded in our earlier work that homolytic bond scissions are not the most important unimolecular decomposition reactions for OMEs [9]. The unimolecular reaction pathways for MMF and FA were extensively searched via exploration of the multidimensional potential energy surface with quantum chemical calculations. The results are depicted by means of schematic potential energy surfaces in Fig. 2. Verification of the transition states was performed via intrinsic reaction coordinate calculations for all reactions.

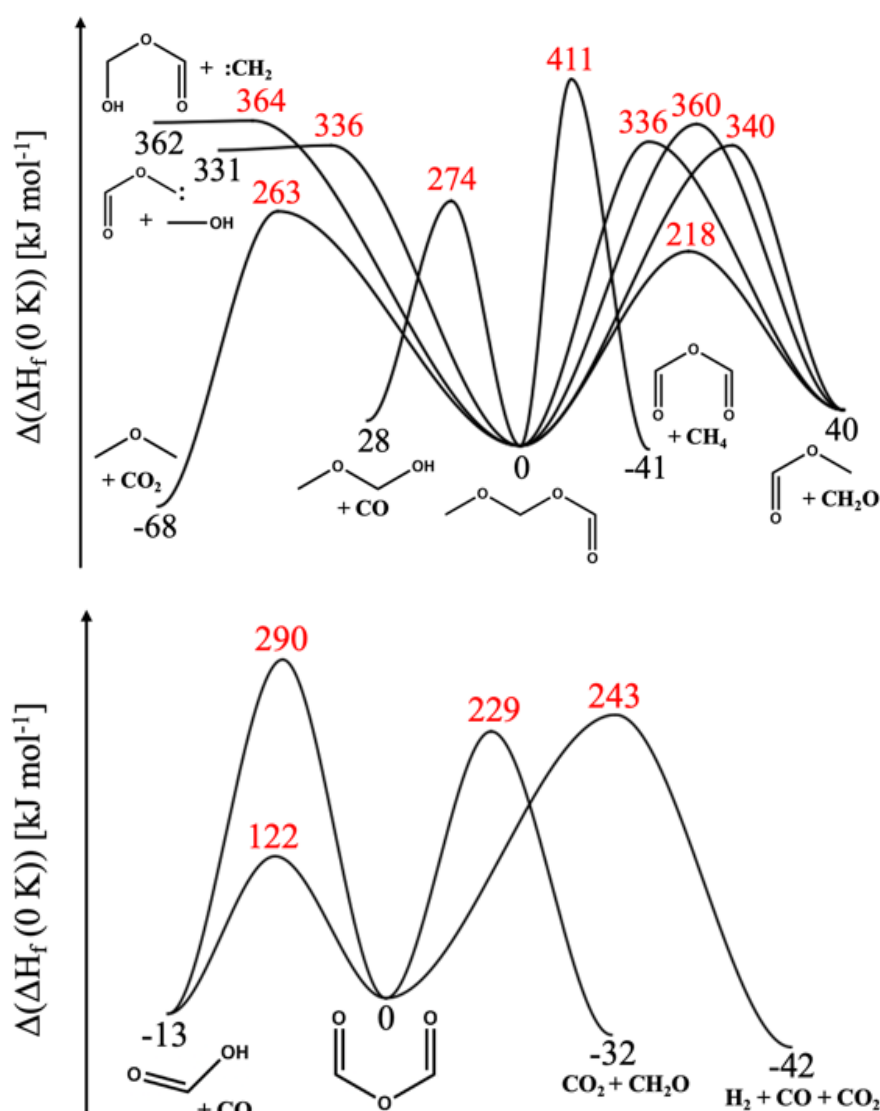


Fig. 2. Schematic potential energy surfaces for unimolecular decomposition of methoxymethyl formate (top) and formic anhydride (bottom). The values are CBS-QB3 calculated enthalpies of formation at 0 K relative to the enthalpy of formation of methoxymethyl formate and formic anhydride, respectively.

In the case of MMF, multiple reaction pathways are available with a significantly lower electronic barrier than the lowest BDE, which amounts to 349 kJ mol⁻¹. The latter is an indication of the energy required for homolytic scission reactions to occur. The lowest electronic barrier of 218 kJ mol⁻¹ is associated with an endothermic elimination reaction forming MF and formaldehyde with the C₂-O₁ bond serving as the source for

the formaldehyde molecule. Three additional formaldehyde eliminations are possible, which differ in the carbon-oxygen bond that is being eliminated, with significantly higher activated ($>100 \text{ kJ mol}^{-1}$) energies for the transition states. The second least activated reaction forms CO_2 and dimethyl ether (DME) with an electronic barrier amounting to 263 kJ mol^{-1} . There is a difference of 45 kJ mol^{-1} in the electronic barrier with the most favorable formaldehyde elimination indicating the dominance of the latter at low temperatures. Due to the stability of DME and CO_2 as products, this reaction is exothermic with an electronic reaction enthalpy of -68 kJ mol^{-1} . The other exothermic reaction forms very stable molecules, i.e., FA and methane, but has the highest electronic reaction barrier, i.e., 411 kJ mol^{-1} . Methoxymethanol and CO can be formed from MMF via an electronic barrier of 274 kJ mol^{-1} . The transition states for the roaming reactions forming carbenes correspond with higher electronic reaction barriers, i.e., 336 and 364 kJ mol^{-1} , and are thus expected to be of minor importance. All these concerted reactions have as a common feature the breaking of two single C-O bonds or one C-O and one C-H bond.

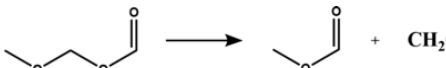
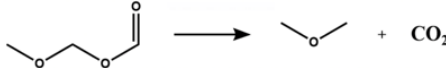
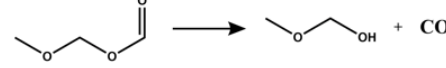
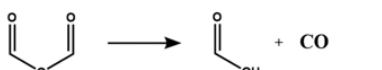
In the case of FA, there are three elementary reactions possible, which are all exothermic and with electronic barriers significantly below the lowest BDE of 391 kJ mol^{-1} . The reaction pathway forming CO and formic acid proceeds via an electronic reaction barrier of only 122 kJ mol^{-1} , which makes FA highly unstable – even under moderate conditions. In the associated transition state, the hydrogen atom of the leaving carbonyl group is transferred to the oxygen atom of the other carbonyl functionality. The same reaction can proceed via another transition state where the hydrogen atom is transferred to the oxygen connecting both carbonyl functionalities, which has a higher electronic reaction barrier of 290 kJ mol^{-1} . Less favorable reaction pathways form CO_2 and formaldehyde or H_2 , CO and CO_2 with electronic barriers of 229 and 243 kJ mol^{-1} ,

respectively. The significant difference in energies of these electronic barriers is confirmed with calculations at other levels of theory.

Modified Arrhenius parameters regressed on the high-pressure limit reaction rate coefficients for the most dominant unimolecular decomposition pathways are listed in Table 1.

Table 1.

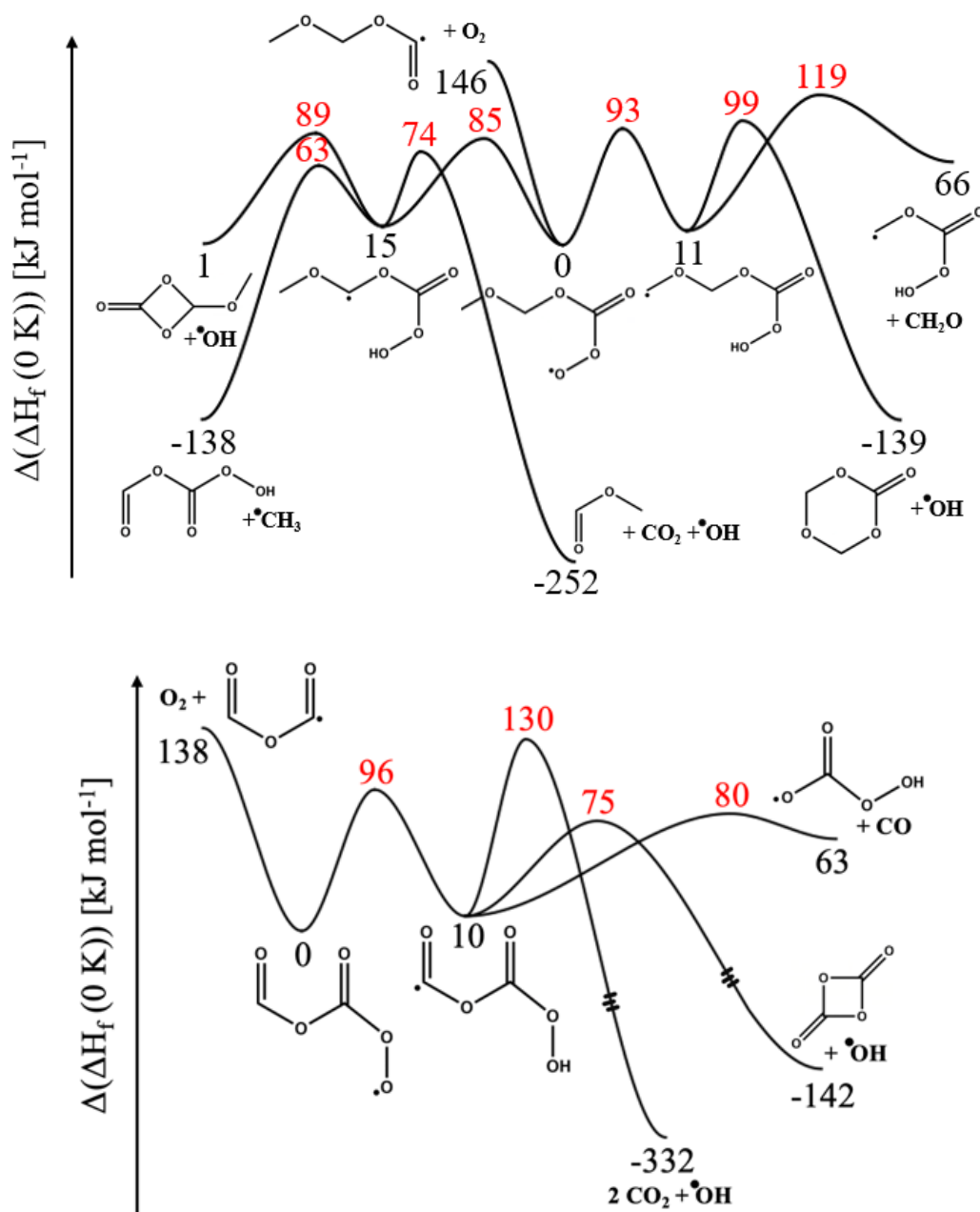
High-pressure limit modified Arrhenius parameters at the CBS-QB3 level of theory for the dominant unimolecular decomposition pathways of methoxymethyl formate and formic anhydride, regressed over the temperature range from 300 to 2000 K.

Reaction	A [s ⁻¹]	n [-]	E_a [kJ mol ⁻¹]
	3.83 E+11	0.724	216.2
	7.57 E+13	0.923	261.8
	1.55 E+11	1.737	267.6
	8.32 E+11	0.354	116.6

3.2. Low-temperature oxidation

In the case that sufficient radicals appear in the reaction environment, these most likely dominate the decomposition due to radical chemistry being associated with significantly lower electronic barriers – due to the unstable nature of radicals – than the aforementioned unimolecular decomposition pathways. Under low-temperature oxidation conditions, the radicals of MMF and FA can interact with molecular oxygen via radical addition reactions. Relevant parts of the potential energy surfaces are depicted in Fig. 3 for the low-temperature decomposition pathways of both the C₁ MMF (CH₃OCH₂OC[•]O, R₁[•]) and the FA (OCHOC[•]O, FA[•]) radical. For the addition of

263 $\text{CH}_3\text{OC}^*\text{HOCHO}$ (R_2^*) and $\text{C}^*\text{H}_2\text{OCH}_2\text{OCHO}$ (R_3^*) to molecular oxygen, the potential
 264 energy surfaces are presented in the Supplementary Material. The names of the radicals
 265 correspond with the nomenclature defined in Fig. 1.



267
 268 **Fig. 3.** Selected part of the potential energy surfaces for the addition of
 269 $\text{CH}_3\text{OCH}_2\text{OC}^*\text{O}$ (top) and OCHOC^*O (bottom) to molecular oxygen. The values are
 270 CBS-QB3 calculated enthalpies of formation at 0 K relative to the enthalpy of formation
 271 of $\text{CH}_3\text{OCH}_2\text{OC}(\text{O})\text{OO}^*$ and $\text{OCHOC}(\text{O})\text{OO}^*$, respectively.

In the case of $\text{CH}_3\text{OCH}_2\text{OC}'\text{O}$, the formation of the C-OO bond via radical addition to molecular oxygen corresponds to an electronic reaction enthalpy of 146 kJ mol^{-1} . The formed peroxy radical can isomerize via two intramolecular hydrogen abstractions. The latter reactions proceed via a six- and eight-membered transition state with an electronic reaction barrier of 85 and 93 kJ mol^{-1} , respectively. These hydroperoxy alkyl radicals can decompose via a β -scission or cyclic ether formation. The formation of the secondary carbon radical, which is 15 kJ mol^{-1} higher in energy, is favored. For this radical, the β -scission forming FA with a hydroperoxide functional group, and the methyl radical is least activated with an electronic barrier of 48 kJ mol^{-1} . Correspondingly, the reaction releases 123 kJ mol^{-1} of energy. The second β -scission forms MF, CO_2 and the hydroxyl radical with an electronic barrier of 59 kJ mol^{-1} and the largest electronic reaction enthalpy of -237 kJ mol^{-1} . The pronounced exothermicity can be explained by the stable nature of the formed products. In the case of cyclic ether formation, the electronic barrier amounts to 74 kJ mol^{-1} , but the reaction enthalpy only amounts to -14 kJ mol^{-1} due to the large ring strain in the cyclic product. This cyclic ether can quickly decompose forming CO_2 and MF. Similarly, the primary carbon radical is 11 kJ mol^{-1} higher in energy than the peroxy radical. For this radical, the cyclic ether formation has the lowest electronic barrier amounting to 88 kJ mol^{-1} and has an electronic reaction enthalpy of -128 kJ mol^{-1} . This six-membered cyclic ether can decompose forming two formaldehyde molecules and CO_2 . In the case of the primary radical, only one β -scission is possible, which is endothermic and corresponds with an electronic barrier of 108 kJ mol^{-1} .


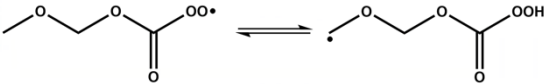

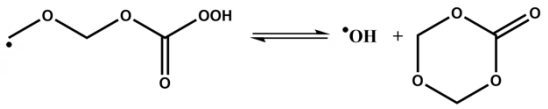
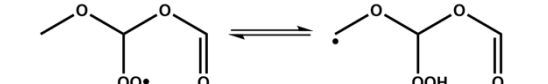
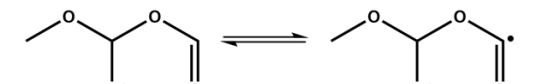
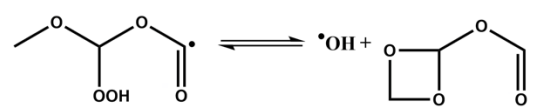
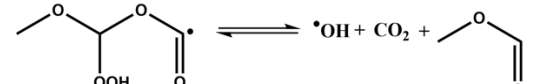
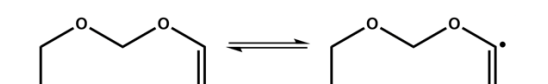
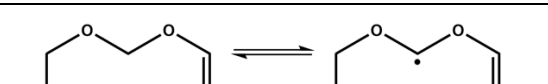
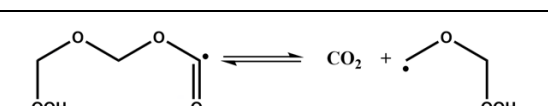

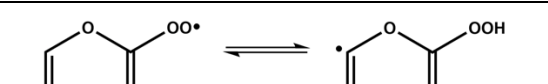
In the case of the radical of FA, the barrierless addition reaction to molecular oxygen has an electronic reaction enthalpy of 138 kJ mol^{-1} . Only one intramolecular hydrogen abstraction with a six-membered transition state can take place, which has an

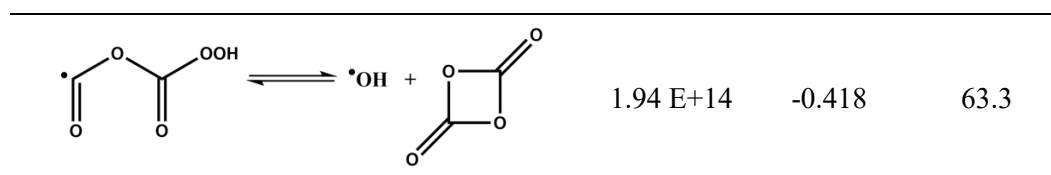
electronic barrier of 96 kJ mol⁻¹. The formed hydroperoxy alkyl radical is 10 kJ mol⁻¹ higher in energy. The formation of a four-membered cyclic ether with two carbonyl functionalities and the hydroxyl radical has the least activated transition state amounting to 65 kJ mol⁻¹. This cyclic ether is very unstable and will quickly decompose forming two CO₂ molecules accompanied by an energy release of 190 kJ mol⁻¹. β -scission of the hydroperoxy alkyl radical is a second decomposition pathway, which creates in a single elementary step two CO₂ molecules and a hydroxyl radical with an electronic reaction enthalpy of -332 kJ mol⁻¹. The corresponding electronic barrier amounts to 120 kJ mol⁻¹. In addition, the endothermic β -scission of the hydroperoxy alkyl radical forming CO and the oxymethylperoxy acid radical (HCO₄•) has an electronic barrier of 70 kJ mol⁻¹. It is noted that the addition of the hydroperoxy alkyl radical of FA to another molecular oxygen does not create extra decomposition pathways, except for intermolecular hydrogen abstraction by the peroxy group, due to missing hydrogen atoms to isomerize.

Modified Arrhenius parameters regressed on the high-pressure limit reaction rate coefficients are listed in **Table 2** for the least activated reaction pathways during low-temperature oxidation of MMF and FA (based on the potential energy surfaces in **Fig. 3** and the ones depicted in the Supplementary Material).

Table 2.

High-pressure limit modified Arrhenius parameters at the CBS-QB3 level of theory for the least activated reaction pathways during low-temperature oxidation of methoxymethyl formate and formic anhydride, regressed over the temperature range from 300 to 2000 K.

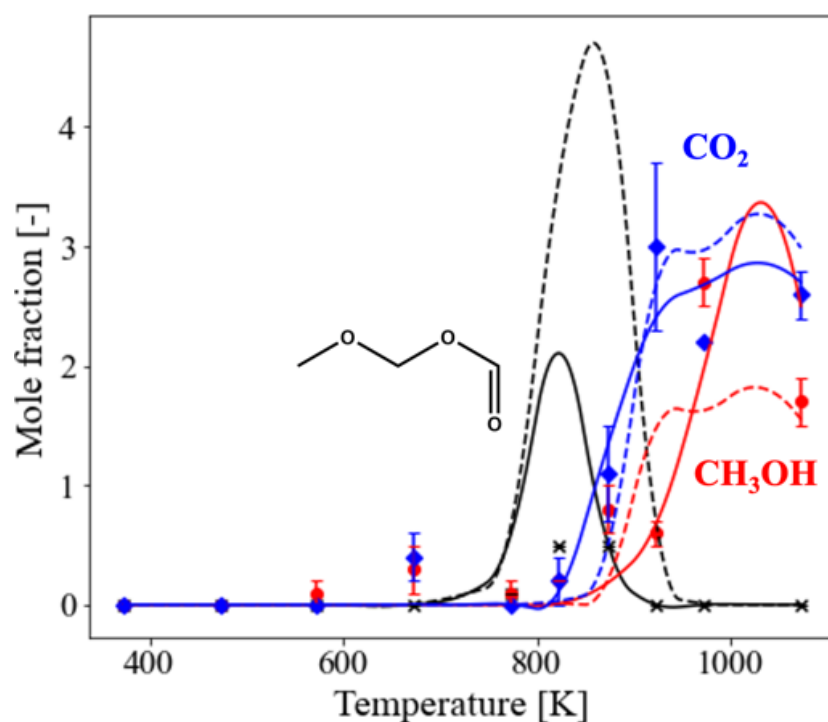
Reaction	<i>A</i> [s ⁻¹]	<i>n</i> [-]	<i>E_a</i> [kJ mol ⁻¹]
	1.66 E+08	1.085	73.3
	1.05 E+04	1.851	69.7
	3.22 E+10	0.893	73.1
	1.82 E+12	-0.235	82.7
	5.93 E+02	2.510	67.4
	3.29 E+07	1.155	72.5
	5.03 E+16	-0.837	87.0
	1.75 E+13	0.006	36.1
	7.76 E+09	0.138	68.1
	1.91 E+09	0.768	75.3
	1.47 E+12	-0.048	50.0
	1.03 E+15	-0.533	90.5
	1.56 E+09	0.818	82.4



322

323 3.3. Kinetic model simulation results

324 Pyrolysis experiments for OME-2 in a tubular quartz reactor [9] have been
 325 simulated with the original and newly developed kinetic model. The experimental
 326 measurements for MMF, methanol and CO₂ are depicted in Fig. 4 and compared with
 327 the predictions from both models. The calculated residence time range amounts to 1.0
 328 to 2.6 s (at 1073 and 373 K, respectively) for the newly developed kinetic model.



329

330 **Fig. 4.** Comparison between experimentally measured (points) and modeled product
 331 yields (lines) [methoxymethyl formate (black), CO₂ (blue), methanol (red)] during
 332 OME-2 pyrolysis as function of the reactor temperature set-point. Full and dashed lines
 333 represent the newly developed and original kinetic model, respectively. Simulations are
 334 performed using the ideal PFR model (length of 120 mm and inner diameter of 4.0 mm)
 335 with an inlet composition of 2.18 mol% OME-2 and 0.02 mol% DMM diluted in helium

at 0.34 MPa and with as input the measured temperature profiles from the original study [9].

For the major products formed during the pyrolysis of OME-2, i.e., CO, H₂, methane and formaldehyde, the change in model performance is not significant and thus not discussed, see the Supplementary Material for the actual comparison. The newly developed model predicts significantly less MMF in line with the experimental yields and the downward trend agrees very well with the measurements. Note that the remaining discrepancies can be related to the experimental uncertainty, the formation chemistry of MMF, as well as the decomposition chemistry of MMF. Only the decomposition chemistry has been looked at in this study. For methanol, the newly developed model also approaches better the experimentally observed trend and reaches a higher maximum in line with the highest measured yield. At around 1100 K, the model predicts the nearly complete conversion of methanol. In the case of CO₂, a better agreement is found for the onset temperature and stagnation at around 2.5 mol% at higher temperatures. FA was not measured during the experiments, but the new model now also predicts a concentration lower than the detection limit. The latter is not the case for the original model.

The newly developed kinetic model can describe the experimental data better compared to the original model, in particular the formation of minor compounds. Since the original model used a lot of analogues from MF and OME-2 which overpredicts the MMF and FA concentrations, it is assumed that MMF and FA are more reactive compounds. The latter is confirmed by the quantum chemical calculations of analogue reactions like β -scissions. For example, consider the lowest electronic reaction barrier for a formaldehyde elimination which amounts to 276 kJ mol⁻¹ in the case of OME-2, while it is only 218 kJ mol⁻¹ for MMF. Simulation results of the newly developed kinetic

model for oxidation experiments with OME-2/air mixtures in a rapid compression machine, at 0.5 and 1.0 MPa and an equivalence ratio amounting to 0.5 (oxygen-rich conditions) [9], are provided in the Supplementary Material. There is no significant difference observed in the model results. The oxidation chemistry of MMF and FA becomes more important for longer chain OMEs as these compounds will be formed more readily after β -scissions of secondary carbon radicals.

3.4. Reaction pathway and sensitivity analysis

A reaction pathway analysis for the formation and decomposition of MMF and FA during the pyrolysis experiments of OME-2 is presented in Fig. 5 for a reactor temperature set-point of 873 K at a pressure of 0.34 MPa. Percentages represent the fraction of the reactant decomposing via the specified pathways at the beginning and the middle of the tubular reactor with associated a measured process gas temperature of 825 and 873 K, respectively.

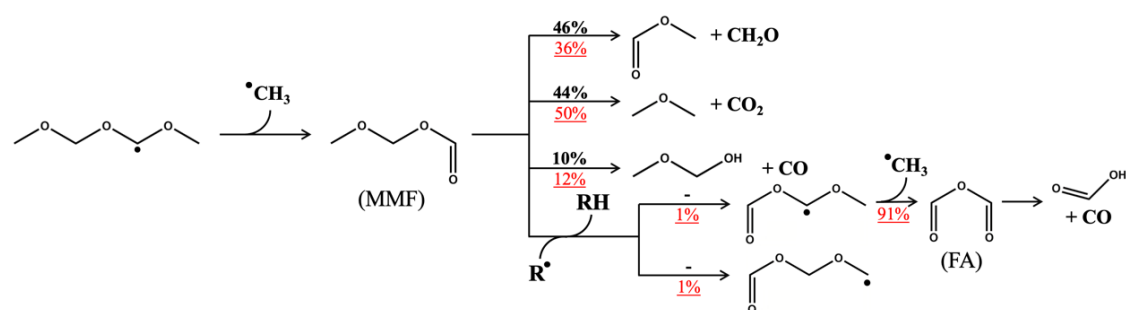


Fig. 5. Reaction pathway analysis obtained with the newly developed kinetic model for the OME-2 pyrolysis experiments in a micro-pyrolysis unit with a reactor temperature set-point of 873 K and pressure of 0.34 MPa. Simulations are performed using the ideal PFR model (length of 120 mm and inner diameter of 4.0 mm) with an inlet composition of 2.18 mol% OME-2 and 0.02 mol% DMM diluted in helium at 0.34 MPa and with as input the measured temperature profiles from the original study [9]. Percentages report the branching fractions via the specified pathways at a distance of 3 cm (bold, black) and 5 cm (underlined, red) along the reactor length.

MMF is only formed after β -scission of the secondary radical of OME-2, also creating the methyl radical. The three included unimolecular reaction pathways for MMF account for most of the decomposition at the investigated reaction conditions. Radical chemistry can only proceed once sufficient radicals are formed in the reaction system. Even though radicals are readily present at a distance of 5 cm along the reactor length, radical chemistry remains unimportant, i.e., merely 2% of the MMF conversion can be attributed to radical chemistry. At a temperature of 825 K (3 cm), formaldehyde elimination of MMF is the most important reaction but in competition with a CO₂ elimination. Despite the significantly lower electronic activation barrier of the formaldehyde elimination, CO₂ elimination becomes more important at higher temperatures due to the entropic contribution. The formation of methoxymethanol and CO from MMF is also responsible for approximately 10% of the decomposition.

Hydrogen abstractions from MMF will create the primary (R₃•) and secondary (R₂•) carbon radical of MMF in equal amounts. Formation of the radical on the carbonyl functionality (R₁•) is less favorable although this is corresponding with the weakest C-H bond in MMF. The dominant radicals in the reaction system are the methyl radical and the hydrogen atom for which all reaction rate coefficients were determined via quantum chemical calculations. R₂• mainly decomposes forming FA and a methyl radical after β -scission. The β -scission forming MF and a formyl radical is less important. The formed FA completely decomposes via fast unimolecular decomposition into formic acid and CO.

The difference in the performance of both kinetic models (c.f. Fig. 4) can thus mainly be explained by the fact that not all unimolecular decomposition pathways for MMF and FA were included and that it did not include accurate kinetic parameters for these species. In the original model, MMF and FA decomposition is mainly predicted

to occur via radical chemistry, which gives rise to a completely different product spectrum.

Note that for larger OMEs, it will be even easier to form MMF during their decomposition since the presence of secondary OME radicals are more abundant than primary carbon radicals. Secondary OME radicals will always create carbonyl functionalities after β -scission. In addition, the simulated pyrolysis experiments are under very dilute conditions (> 97.5 mol% inert) and thus favor the unimolecular decomposition pathways. At conditions with less dilution, i.e., conditions that favor bimolecular reactions, the formation of MMF and FA as intermediates will be more pronounced. This has been confirmed with unpublished pyrolysis experiments for OME-2 in a different experimental unit with a dedicated analysis section under less diluted conditions, during which more MMF is formed, and FA and formic acid could be detected and quantified.

The results of a sensitivity analysis under pyrolysis conditions are presented in Fig. 6 for MFF by means of the normalized sensitivity coefficients for the most sensitive reactions. MMF is only formed after a β -scission of the secondary carbon radical of OME-2 and therefore the only reaction to increase its formation. The competing β -scission to form methyl formate and the methoxymethyl radical is inhibiting the formation in a similar proportion. Moreover, the most favorable unimolecular decomposition reactions of MMF are also sensitive as they can directly convert MMF and affect the molar yield.

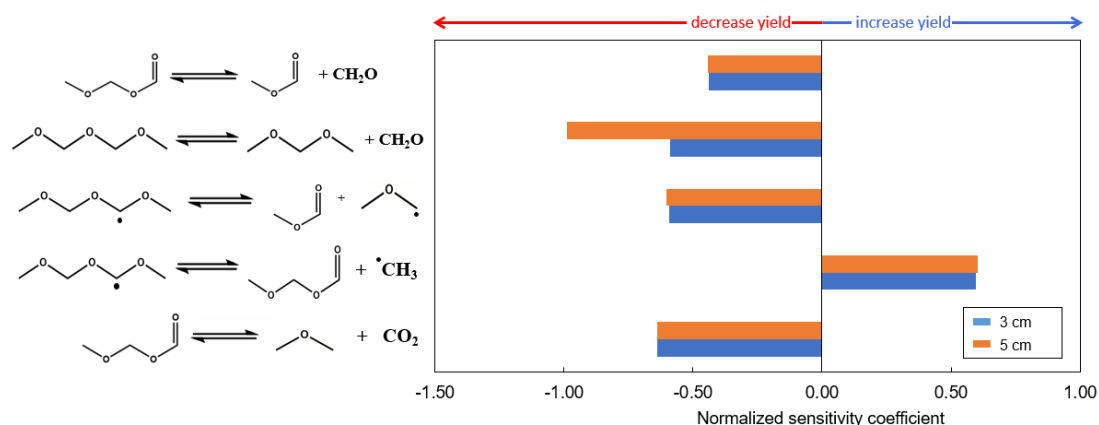


Fig. 6. Normalized sensitivity coefficients on the mole fraction of methoxymethyl formate during OME-2 pyrolysis. Experimental conditions correspond to a pressure of 0.34 MPa and a reactor temperature set-point of 873 K at 3.00 (blue) and 5.00 cm (orange) along the reactor.

The results of the sensitivity analysis for FA are analogously depicted in Fig. 7. The unimolecular decomposition reaction of FA is the most sensitive reaction (at 3 cm) as it directly affects the FA yield. The other most sensitive reactions are not directly related to FA itself but to its formation pathways and the creation of radicals in the reaction system. Formaldehyde elimination of OME-2 strongly inhibits the formation of FA as it does compete with the carbene pathways forming radicals, and dimethyl ether cannot lead to the formation of MMF. Reactions leading to the formation of MMF directly favor FA formation. The most sensitive reactions for MMF and FA are therefore very similar.

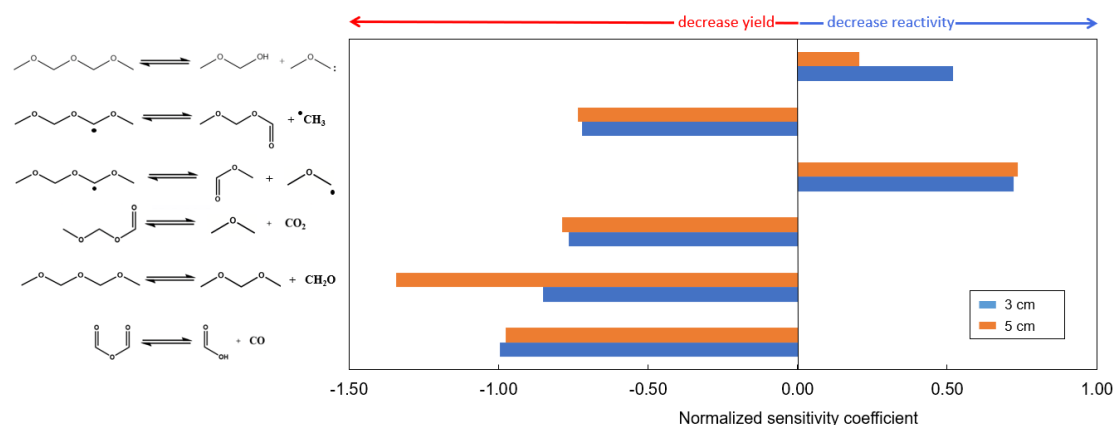


Fig. 7. Normalized sensitivity coefficients on the mole fraction of formic anhydride during OME-2 pyrolysis. Experimental conditions correspond to a pressure of 0.34 MPa and a reactor temperature set-point of 873 K at 3.00 (blue) and 5.00 cm (orange) along the reactor.

4. Conclusions

A comprehensive study on the pyrolysis and combustion of MMF and FA has been performed by means of combined theoretical calculations and kinetic modeling to better understand the secondary chemistry of OMEs. Electronic structure calculations at the CBS-QB3 level of theory are used to calculate thermodynamic parameters and high-pressure limit reaction rate coefficients for MMF and FA specific reactions. A new kinetic model is developed based on first principles to describe the pyrolysis and combustion of MMF and FA. Validation of the model is performed with OME-2 pyrolysis experiments during which MMF is formed as an intermediate and RCM experiments. The new kinetic model predicts the experimental trends well and in particular minor species yields are in line with the 10 mol% rel. uncertainty margin. MMF and FA are found to be more reactive compared to their OME analogue. A reaction pathway analysis indicated that MMF and FA mainly decompose via unimolecular decomposition pathways under pyrolysis conditions, i.e., formaldehyde and CO₂ eliminations in the case of MMF and CO elimination in the case of FA. Radical

chemistry does only contribute marginally to the decomposition under dilute conditions. This MMF and FA decomposition chemistry is now available for the development of detailed kinetic models for larger OMEs in our next studies.

Declaration of competing interest

The authors declare that they have no known competing financial interests or personal relationships that could have appeared to influence the results reported in this paper.

Acknowledgments

The computational resources and services used for this work were provided by the Flemish Supercomputer Center (VSC), funded by the Fund for Scientific Research Flanders (FWO) and the Flemish Government department EWI. Kevin De Ras and Mike Bonheure acknowledge the Fund for Scientific Research Flanders (FWO) for financial support via doctoral fellowship grants 3F018119 and 1SD7121N, respectively. The research leading to these results has also received funding from the European Research Council under the European Union's Horizon 2020 research and innovation programme / ERC grant agreement n° 818607.

Supplementary material

A separate Word document (.docx) is provided containing a list containing all new thermodynamic parameters and modified Arrhenius parameters calculated at the CBS-QB3 level of theory, the geometrical structures for species and transition states, the remaining potential energy surfaces with discussion and the comparison of experimental measurements with model predictions for major products. The developed kinetic model is provided in CHEMKIN format (.inp).

References

- [1] K.M. Van Geem, B.M. Weckhuysen, Toward an e-chemistree: Materials for electrification of the chemical industry, *MRS bulletin* 46 (2021).
- [2] D. Pélerin, K. Gaukel, M. Härtl, E. Jacob, G. Wachtmeister, Potentials to simplify the engine system using the alternative diesel fuels oxymethylene ether OME1 and OME3–6 on a heavy-duty engine, *Fuel* 259 (2020) 116231.
- [3] K. De Ras, R. Van de Vijver, V.V. Galvita, G.B. Marin, K.M. Van Geem, Carbon capture and utilization in the steel industry: challenges and opportunities for chemical engineering, *Current Opinion in Chemical Engineering* 26 (2019) 81-87.
- [4] S. Schemme, R.C. Samsun, R. Peters, D. Stolten, Power-to-fuel as a key to sustainable transport systems – An analysis of diesel fuels produced from CO₂ and renewable electricity, *Fuel* 205 (2017) 198-221.
- [5] A. Omari, B. Heuser, S. Pischinger, C. Rüdinger, Potential of long-chain oxymethylene ether and oxymethylene ether-diesel blends for ultra-low emission engines, *Applied Energy* 239 (2019) 1242-1249.
- [6] J.K. Mwangi, W.-J. Lee, Y.-C. Chang, C.-Y. Chen, L.-C. Wang, An overview: Energy saving and pollution reduction by using green fuel blends in diesel engines, *Applied Energy* 159 (2015) 214-236.
- [7] J. Benajes, A. García, J. Monsalve-Serrano, R. Sari, Clean and efficient dual-fuel combustion using OMEx as high reactivity fuel: Comparison to diesel-gasoline calibration, *Energy Conversion and Management* 216 (2020) 112953.
- [8] J. Liu, H. Wang, Y. Li, Z. Zheng, Z. Xue, H. Shang, M. Yao, Effects of diesel/PODE (polyoxymethylene dimethyl ethers) blends on combustion and emission characteristics in a heavy duty diesel engine, *Fuel* 177 (2016) 206-216.
- [9] K. De Ras, M. Kusenberg, G. Vanhove, Y. Fenard, A. Eschenbacher, R.J. Varghese, J. Aerssens, R. Van de Vijver, L.-S. Tran, J.W. Thybaut, K.M. Van Geem, A detailed experimental and kinetic modeling study on pyrolysis and oxidation of oxymethylene ether-2 (OME-2), *Combustion and Flame* 238 (2022)

111914.

[10] J.S. Francisco, Mechanistic Study of the Gas-Phase Decomposition of Methyl Formate, *Journal of the American Chemical Society* 125 (2003) 10475-10480.

[11] S. Dooley, M.P. Burke, M. Chaos, Y. Stein, F.L. Dryer, V.P. Zhukov, O. Finch, J.M. Simmie, H.J. Curran, Methyl formate oxidation: Speciation data, laminar burning velocities, ignition delay times, and a validated chemical kinetic model, *International Journal of Chemical Kinetics* 42 (2010) 527-549.

[12] M.U. Alzueta, V. Aranda, F. Monge, Á. Millera, R. Bilbao, Oxidation of methyl formate and its interaction with nitric oxide, *Combustion and flame* 160 (2013) 853-860.

[13] W. Ren, E. Dames, D. Hyland, D.F. Davidson, R.K. Hanson, Shock tube study of methanol, methyl formate pyrolysis: CH₃OH and CO time-history measurements, *Combustion and flame* 160 (2013) 2669-2679.

[14] W.K. Metcalfe, S.M. Burke, S.S. Ahmed, H.J. Curran, A Hierarchical and Comparative Kinetic Modeling Study of C1 – C2 Hydrocarbon and Oxygenated Fuels, *International Journal of Chemical Kinetics* 45 (2013) 638-675.

[15] E. Ranzi, A. Frassoldati, A. Stagni, M. Pelucchi, A. Cuoci, T. Faravelli, Reduced Kinetic Schemes of Complex Reaction Systems: Fossil and Biomass-Derived Transportation Fuels, *International Journal of Chemical Kinetics* 46 (2014) 512-542.

[16] L. Cai, S. Jacobs, R. Langer, F. vom Lehn, K.A. Heufer, H. Pitsch, Auto-ignition of oxymethylene ethers (OMEn, n = 2–4) as promising synthetic e-fuels from renewable electricity: shock tube experiments and automatic mechanism generation, *Fuel* 264 (2020) 116711.

[17] T. He, Z. Wang, X. You, H. Liu, Y. Wang, X. Li, X. He, A chemical kinetic mechanism for the low- and intermediate-temperature combustion of Polyoxymethylene Dimethyl Ether 3 (PODE3), *Fuel* 212 (2018) 223-235.

[18] W. Sun, G. Wang, S. Li, R. Zhang, B. Yang, J. Yang, Y. Li, C.K. Westbrook, C.K. Law, Speciation and the laminar burning velocities of poly(oxymethylene)

547 dimethyl ether 3 (POMDME3) flames: An experimental and modeling study,
 548 Proceedings of the Combustion Institute 36 (2017) 1269-1278.

549 [19] J.A.M. Jr., M.J. Frisch, J.W. Ochterski, G.A. Petersson, A complete basis set
 550 model chemistry. VI. Use of density functional geometries and frequencies, The
 551 Journal of Chemical Physics 110 (1999) 2822-2827.

552 [20] M.J. Frisch, G.W. Trucks, H.B. Schlegel, G.E. Scuseria, M.A. Robb, J.R.
 553 Cheeseman, G. Scalmani, V. Barone, G.A. Petersson, H. Nakatsuji, X. Li, M.
 554 Caricato, A.V. Marenich, J. Bloino, B.G. Janesko, R. Gomperts, B. Mennucci,
 555 H.P. Hratchian, J.V. Ortiz, A.F. Izmaylov, J.L. Sonnenberg, Williams, F. Ding, F.
 556 Lipparini, F. Egidi, J. Goings, B. Peng, A. Petrone, T. Henderson, D. Ranasinghe,
 557 V.G. Zakrzewski, J. Gao, N. Rega, G. Zheng, W. Liang, M. Hada, M. Ehara, K.
 558 Toyota, R. Fukuda, J. Hasegawa, M. Ishida, T. Nakajima, Y. Honda, O. Kitao,
 559 H. Nakai, T. Vreven, K. Throssell, J.A. Montgomery Jr., J.E. Peralta, F. Ogliaro,
 560 M.J. Bearpark, J.J. Heyd, E.N. Brothers, K.N. Kudin, V.N. Staroverov, T.A.
 561 Keith, R. Kobayashi, J. Normand, K. Raghavachari, A.P. Rendell, J.C. Burant,
 562 S.S. Iyengar, J. Tomasi, M. Cossi, J.M. Millam, M. Klene, C. Adamo, R. Cammi,
 563 J.W. Ochterski, R.L. Martin, K. Morokuma, O. Farkas, J.B. Foresman, D.J. Fox,
 564 Gaussian 16 Rev. C.01, Wallingford, CT, 2016.

565 [21] R. Van de Vijver, K.M. Van Geem, G.B. Marin, On-the-fly ab initio calculations
 566 toward accurate rate coefficients, Proceedings of the Combustion Institute 37
 567 (2019) 283-290.

568 [22] A.L.L. East, L. Radom, Ab initio statistical thermodynamical models for the
 569 computation of third-law entropies, The Journal of Chemical Physics 106 (1997)
 570 6655-6674.

571 [23] L.A. Curtiss, K. Raghavachari, P.C. Redfern, J.A. Pople, Assessment of
 572 Gaussian-2 and density functional theories for the computation of enthalpies of
 573 formation, The Journal of Chemical Physics 106 (1997) 1063-1079.

574 [24] C. Pappijn, F. Vermeire, R. Van de Vijver, M.F. Reyniers, G. Marin, K. Van
 575 Geem, Bond additivity corrections for CBS-QB3 calculated standard enthalpies

- of formation of H, C, O, N, and S containing species, *International Journal of Chemical Kinetics* 53 (2020).
- [25] G.A. Petersson, D.K. Malick, W.G. Wilson, J.W. Ochterski, J.A. Montgomery Jr, M.J. Frisch, Calibration and comparison of the Gaussian-2, complete basis set, and density functional methods for computational thermochemistry, *The Journal of chemical physics* 109 (1998) 10570-10579.
- [26] C. Eckart, The Penetration of a Potential Barrier by Electrons, *Physical Review* 35 (1930) 1303-1309.
- [27] J. Aerssens, F. Vermeire, S.U. Aravindakshan, R. Van de Vijver, K.M. Van Geem, The Merit of Pressure Dependent Kinetic Modelling in Steam Cracking, *Faraday Discussions*, doi:10.1039/D2FD00032F(2022).
- [28] P.D. Paraskevas, M.K. Sabbe, M.F. Reyniers, N. Papayannakos, G.B. Marin, Group additive values for the gas-phase standard enthalpy of formation, entropy and heat capacity of oxygenates, *Chemistry—A European Journal* 19 (2013) 16431-16452.
- [29] H.-H. Carstensen, A.M. Dean, Rate constant rules for the automated generation of gas-phase reaction mechanisms, *The Journal of Physical Chemistry A* 113 (2009) 367-380.
- [30] A.G. Vandeputte, M.K. Sabbe, M.-F. Reyniers, V. Van Speybroeck, M. Waroquier, G.B. Marin, Theoretical study of the thermodynamics and kinetics of hydrogen abstractions from hydrocarbons, *The Journal of Physical Chemistry A* 111 (2007) 11771-11786.
- [31] N. Vandewiele, K. Van Geem, M.-F. Reyniers, B. Marin, Genesys: Kinetic model construction using chemo-informatics, *Chemical Engineering Journal* 207–208 (2012) 526–538.
- [32] L. Cai, H. Pitsch, S.Y. Mohamed, V. Raman, J. Bugler, H. Curran, S.M. Sarathy, Optimized reaction mechanism rate rules for ignition of normal alkanes, *Combustion and Flame* 173 (2016) 468-482.
- [33] R.J. Kee, F.M. Rupley, E. Meeks, J.A. Miller, CHEMKIN-III: A FORTRAN

605 chemical kinetics package for the analysis of gas-phase chemical and plasma
606 kinetics, United States, 1996.
607